ACS SENSORS

pubs.acs.org/acssensors Article

Ultrahigh-Throughput, Real-Time Flow Cytometry for Rare Cell Quantification from Whole Blood

Mahmut Kamil Aslan, Yingchao Meng, Yanan Zhang, Tobias Weiss, Stavros Stavrakis,* and Andrew J. deMello*

Cite This: *ACS Sens.* 2024, 9, 474−482 Read Online

ACCESS | Metrics & More | Article Recommendations | Supporting Information

ABSTRACT: We present an ultrahigh-throughput, real-time fluorescence cytometer comprising a viscoelastic microfluidic system and a complementary metal−oxide-semiconductor (CMOS) linear image sensor-based detection system. The flow cytometer allows for real-time quantification of a variety of fluorescence species, including micrometer-sized particles and cells, at analytical throughputs in excess of 400,000 species per second. The platform integrates a custom C++ control program and graphical user interface (GUI) to allow for the processing of raw signals, adjustment of processing parameters, and display of fluorescence intensity histograms in real time. To demonstrate the efficacy of the platform for rare event detection and its utility as a basic clinical tool, we measure and quantify patient-derived circulating tumor cells (CTCs) in peripheral blood, realizing that detection has a sensitivity of 6 CTCs per million blood cells (0.000006%) with a volumetric throughput of over 3 mL/min.

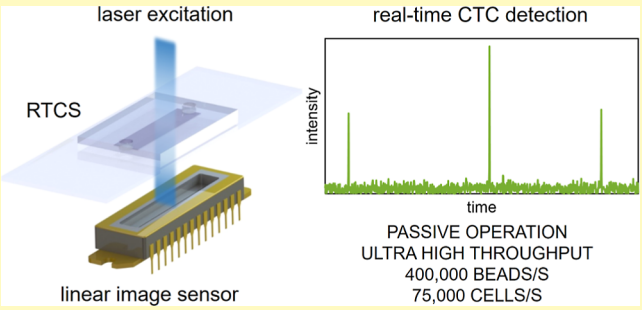

KEYWORDS: *flow cytometry, high-throughput, microfluidics, fluorescence, real-time, circulating tumor cells*

Downloaded via ETH ZURICH on January 31, 2024 at 13:55:41 (UTC).
See https://pubs.acs.org/sharingguidelines for options on how to legitimately share published articles.

Liquid biopsy, an emerging tool in modern oncology, is in principle a minimally invasive diagnostic method for the identification and isolation of circulating tumor biomarkers in various bodily fluids.[1] The most investigated biomarkers in liquid biopsies are circulating tumor cells (CTCs), extracellular vesicles (EVs), and cell-free nucleic acids.[2] It is well recognized that the enumeration of CTCs is correlated with cancer progression[3] and metastasis[4] and, as such, is an important biomarker for the early diagnosis, monitoring, and prognosis of the disease. CTCs were first discovered in patients with breast, lung, pancreatic, prostate, liver, and colon cancers 150 years ago.[5,6] Unsurprisingly, CTC detection can significantly impact not only the early detection of cancer but also its clinical treatment and management.[7,8] Unfortunately, CTCs are extremely rare in number when compared to other cells in whole blood, being found in quantities as low as 1−10 CTCs per billion blood cells.[9] Accordingly, the development of quantitative tools for CTC detection is immensely challenging.[10] A number of different microfluidic tools for CTC detection have been reported in recent years. These include techniques centered on size-based filtration,[11,12] immunomagnetic enrichment,[13,14] or antibody immobilization.[10,15,16] However, almost all of these techniques require an initial enrichment step to enhance sensitivity. Additionally, fluorescence imaging techniques used for CTC detection generally take long time periods and require manual confirmation of detected CTCs.[17,18] In this regard, it is important to note that flow cytometry (FC) can be used to detect CTCs.[19,20]

FC is a high-throughput technique for probing single cells based on their physical and chemical characteristics, and thus in principle could be used in liquid biopsy applications to detect CTCs.[21] It is widely recognized as the gold standard method for quantifying the number, size, size distribution, shape, and morphology of cells within large and heterogeneous populations.[22] In its simplest embodiment, a flow cytometer consists of a hydrodynamic system to focus cells into a single file, an optical detector, and a signal processing system. Integration of all three components enables a large number of cells to be focused and interrogated with electromagnetic radiation of various wavelengths. Typically, forward scatter, side scatter, and fluorescence signals generated by cells as they transit the optical probe volume are detected using photomultiplier tubes (PMTs) or avalanche photodiodes (APDs)[23] and converted to electronic signals. Quantitative information regarding cell size, population size distribution, granularity, shape, and cell content is then extracted and used to

Received: October 26, 2023
Revised: December 8, 2023
Accepted: December 14, 2023
Published: January 3, 2024

© 2024 American Chemical Society

https://doi.org/10.1021/acssensors.3c02268
ACS Sens. 2024, 9, 474−482

characterize the sample under study. In conventional FC, cells are focused into a single file by enveloping the sample stream inside a rapidly moving sheath fluid, with volumetric flow rates typically varying between 10 and 100 μL/min for the sample and between 100 and 700 μL/min for the sheath flow. Such flow rates allow the processing and analysis of cells at rates between 10,000 and 50,000 events/s, depending on sample concentration.[24] Despite the fact that FC is highly efficient at enumerating large numbers of cells in short periods of time, conventional flow cytometers are bulky, costly (to both purchase and run), and commonly require a trained specialist for operation.[25] These features mean that FC is normally performed within a dedicated (central) facility, and although portable flow cytometers do exist,[26] FC is rarely used as an analytical tool outside of the lab, for example, in resource-limited settings where its use in clinical diagnostics would be invaluable. Additionally, most commercial flow cytometers are unsuitable for the detection of CTCs, due to their low operational volumetric throughput rates, typically between 10 and 100 μL/min[27] In addition, sample processing times, including pre-enrichment steps and acquisition, can be excessively long, taking more than 24 h per sample.[28]

In recent years, microfluidic-based flow cytometers have been used to quantify both particle and cellular populations.[29] Compared to their conventional counterparts, microfluidic flow cytometers have several advantageous features, including reduced reagent consumption, portability, and lower unit costs.[30] Importantly, they can also be integrated with other microfluidic devices to automate FC workflows, including sample preparation processes, such as antibody incubation and cell staining.[31] All these features point toward a new generation of portable yet powerful and simple-to-use flow cytometers for point-of-care or in-the-field applications. Additionally, it should be noted that microfluidic flow cytometers can operate at exceptionally high throughput by taking advantage of both hydrodynamic (e.g., inertial) effects[32] and parallelization.[33] This means that in principle, microfluidic cytometers can be used to quantify rare cells within large heterogeneous populations; a task that typically takes unacceptably long processing times using commercial flow cytometers.[27] Many microfluidic cytometers mimic conventional flow cytometers in terms of their structure and operation, with cells being focused on a single file using a sheath flow.[34,35] Sheath flows are useful at both focusing cells into flow in a narrow core stream and reducing the possibility of multiple cells entering the detection area at the same time. Such coincidences occur when two or more cells occupy (or partially occupy) the detection volume simultaneously,[36] and lead to convoluted signals. While sheath flows are effective in aligning cells, they involve complex fluidic control operations and consume significant amounts of sheath fluid. This not only dilutes the particle or cell concentration (thus limiting analytical throughput) but also drastically increases the reagent costs. Accordingly, "sheathless" cell focusing methods have attracted interest. For example, dielectrophoretic forces can be used to manipulate and focus dielectric particles through the application of nonuniform electric fields.[37] Although dielectrophoretic focusing has been shown to be valuable in enriching particles or cells, dielectrophoretic systems are complex to both fabricate and control and operate at relatively low analytical throughputs.[38] Acoustic actuation can also be used to focus cells within chip-based flow cytometers. Here, cells are driven toward pressure nodes or antinodes depending on the relative compressibility of the cell and suspension medium.[39] Acoustic focusing can be achieved by actuating a piezoelectric material with traveling surface acoustic waves (TSAWs)[40] or standing surface acoustic waves (SSAWs).[41] Acoustic particle manipulation has many desirable features, such as being label-free, noncontact, and biocompatible. However, acoustic components comprise complex electrode geometries and sophisticated control equipment. Accordingly, to address the aforementioned issues, inertial and elasto-inertial microfluidic systems have been used for single-cell focusing. Such approaches are desirable since they operate in a passive and high-throughput manner and only require simple channel structures.[42−44] The use of elasto-inertial phenomena to focus and position cells is of particular interest since efficient 3-D focusing of micron-sized species can be achieved within simple microfluidic circuits at relatively low flow rates.[45,46] These features suggest that elasto-inertial focusing holds great potential in realizing a new generation of cost-effective, high-throughput, and portable flow cytometers.[47]

Microfluidic flow cytometers leverage a variety of detection approaches based on both electrical and optical signals.[31,48] Of these, fluorescence-based detection methods are the most popular. They are exquisitely sensitive and allow multiple parameters to be analyzed simultaneously.[35] Unsurprisingly, laser-induced fluorescence (LIF) is a universally adopted detection method in both commercial and chip-based flow cytometers.[49] LIF involves the excitation of (intrinsic or extrinsic) fluorophores located within or on the surfaces of cells. Fluorescence photons are subsequently collected using integrated or free-space optics and detected using charge-coupled devices (CCDs), APDs, or PMTs. In recent years, CMOS image sensors have also been used in flow cytometers due to their low cost, high-speed operation, and large fields of view. To date, a number of microfluidic flow cytometers incorporating fluorescence detection have been reported in the literature. For example, Fan et al. reported a high throughput multicolor fluorescence cytometer integrating sheath flow focusing.[50] The system includes a multilayer microfluidic device able to perform parallel 3D flow focusing and fluorescence detection in 32 channels with a maximum theoretical throughput of 10^6 cells/s. Unfortunately, volumetric throughput was limited to 0.33 mL/min. This means that a concentration of 2×10^8 cells/mL would be required to realize a throughput of 10^6 cells/s; an unfeasible concentration in most biological assays. Additionally, Zhao and colleagues developed a fluorescence counting method for CTC screening in blood.[7] Here, peripheral blood was directly labeled with multiple antibodies (conjugated to different fluorophores), pumped through a microfluidic channel, and interrogated via line-confocal fluorescence microscopy. Multiple APDs were subsequently used to detect CTCs at concentrations ranging from 15 to 3375 cells per 1 mL of whole blood. Despite its utility, the maximum volumetric throughput in this system was 80 μL/min, a value insufficient for processing large volumes of blood samples. Many other fluorescence-based microfluidic cytometers rely on the use of conventional microscopes coupled to high-speed cameras[51] or complex optical detection systems.[52] In addition, lens-free holographic on-chip cytometers while being simple in construction[53,54] have generally been applied to the analysis of static suspensions and involve significant computational processing, thus limiting analytical throughput.[55] Accordingly, there remains an unmet need for

https://doi.org/10.1021/acssensors.3c02268
ACS Sens. 2024, 9, 474−482

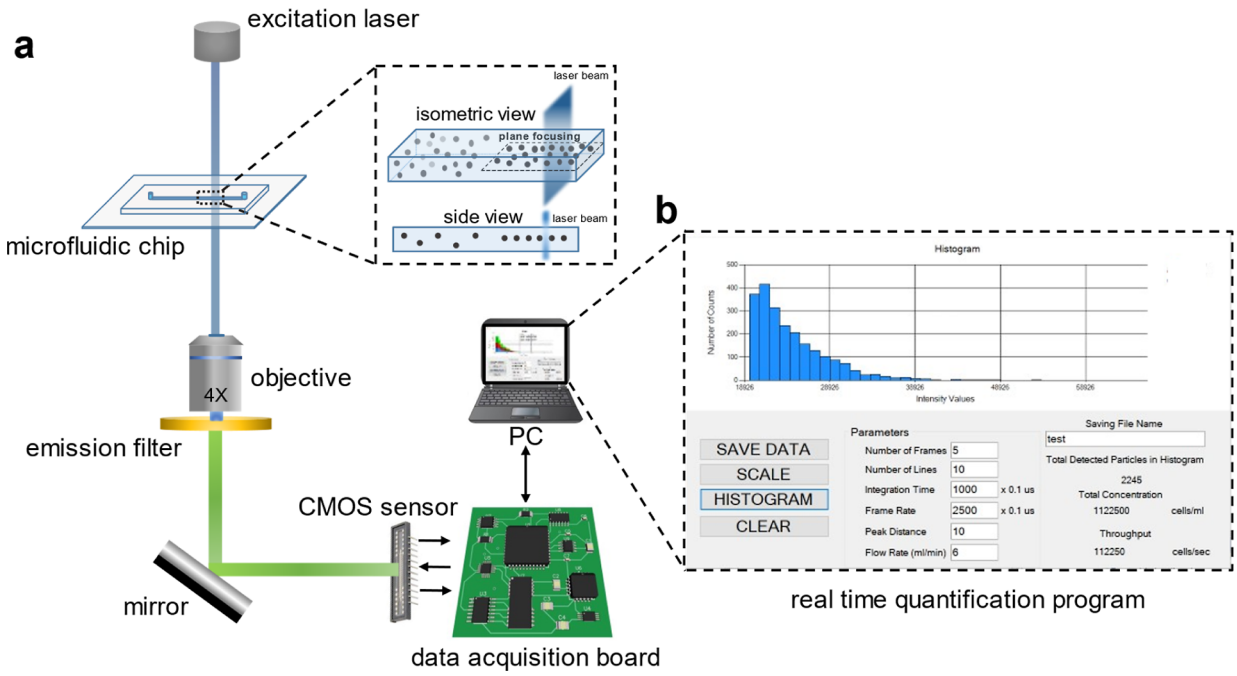

Figure 1. RTCS. (a) Schematic of the RTCS, incorporating a microfluidic device for passive focusing of cells using a viscoelastic fluid, a 488 nm laser, a 4×/0.13 N.A. objective, a 530 nm emission filter with a dichroic mirror (470−490 nm reflection/508−675 nm transmission bands) and a CMOS linear image sensor with the readout circuitry for acquiring and transferring frame data. (b) Screenshot of the real-time signal processing and quantification program. The custom-written program (developed in C++) can acquire and process raw sensor data and display intensity histograms in real time and at a rate of up to 400,000 events/second.

portable, easy-to-use, and high-throughput systems for real-time fluorescence FC.

To this end, we present a microfluidic flow cytometer for quantitative analysis of large populations of cells and particles. Our real-time fluorescence counting system (RTCS) consists of a planar microfluidic device, a CMOS linear image sensor, a simple optical setup for light collection and control electronics (Figure 1). In brief, cells are passively manipulated and focused to a single plane within a microfluidic channel using elasto-inertial forces and subsequently imaged using a CMOS sensor. Fluorescence signals are acquired using a commercial readout circuit and processed in real time using a custom-written C++ program. The presented system offers new opportunities for the real-time and sensitive quantification of large populations of fluorescence particles and cells.

■ MATERIALS AND METHODS

Design and Fabrication of the Microfluidic Device. The microfluidic device integrates a rectangular cross-section microchannel that is 50 mm long, 5 mm wide, and 50 μm deep. Such a low aspect ratio, rectangular cross-section microchannel allows for the focusing of cells (with a mean diameter of 12 μm) in the image plane.[47] Channel designs were drawn using AutoCAD 2019 (Autodesk, San Rafael, USA) and printed onto photolithographic masks (Micro Lithography Services Ltd., Chelmsford, UK). Standard photolithographic techniques were used to fabricate an SU-8 master mold. First, the SU-8 2010 photoresist (Micro Resist Technology, Berlin, Germany) was spin-coated onto a 5 in. diameter silicon wafer (Siegert wafer GmbH, Aachen, Germany). A spin speed of 2000 rpm resulted in a 25 μm thick resist layer. The spin-coated wafer was baked on a 65 °C hot plate for 1 min and a 95 °C hot plate for 4 min. Then, channel patterns in the mask were transferred to the wafer via exposure to UV radiation for 30 s. After exposure, the wafer was baked on a 95 °C hot plate for 4 min to facilitate cross-linking of the exposed SU-8 photoresist. The patterned structures were developed in an mr-Dev 600 Developer solution (Micro Resist Technology, Berlin, Germany), allowing the removal of the unexposed resist. Finally, the wafer was rinsed with isopropyl alcohol and water, followed by drying using pressured air. The fabricated mold was hard-baked on a 150 °C hot plate for 10 min.

Microfluidic devices were fabricated by using standard soft lithography methods. First, the mold was placed into a desiccator containing chlorotrimethylsilane (Sigma-Aldrich, Buchs, Switzerland) for 2 h at a pressure of 150 mbar. A PDMS mixture was then prepared using a 10/1 (w/w) ratio of PDMS base to curing agent (Sylgard 184, Dow Corning, Midland, USA). This mixture was poured onto the mold, degassed in the desiccator for 30 min, and cured overnight in an oven set at 70 °C. The cured PDMS was then peeled off the mold, and individual devices were formed by dicing. Inlet and outlet ports (0.76 mm diameter) were opened by using a hole puncher (Syneo, West Palm Beach, USA). Devices were bonded to planar glass slides (Menzel-Glaser, Braunschweig, Germany) after exposing all surfaces to an oxygen plasma (EMITECH K1000X, Quorum Technologies, Laughton, United Kingdom) for 1 min. Finally, bonded devices were left on a hot plate at 120 °C for 2 h to strengthen the bond.

Cell Preparation. HEK293T Flp-in T-REX cells expressed with a stably integrated mNeonGreen transgene (293T Flp-in T-REX mNeonGreen from Dr. B. Mateescu, University of Zürich) were cultured in DMEM medium (Life Technologies, Zug, Switzerland), supplemented with Glutamax (Life Technologies, Zug, Switzerland), 10% (v/v) fetal bovine serum (FBS, Life Technologies, Zug, Switzerland), and 1% (v/v) penicillin−streptomycin (10,000 U/mL, Life Technologies, Zug Switzerland) at 37 °C and 5% CO_2 (New Brunswick Galaxy 170 S, Eppendorf, Schönenbuch, Switzerland). All experiments were performed on cells in their exponential (log) phase of growth. Two days before experiment, 6 million cells were seeded in a 10 cm diameter plate in the presence of 2 μg/mL doxycycline (Sigma-Aldrich, Buchs, Switzerland) to induce expression of the mNeonGreen protein. Afterward, adherent cells were trypsinized, and the corresponding cell suspension was washed once in PBS.

The human glioblastoma cell line, LN229, was cultured in DMEM medium (Life Technologies, Zug, Switzerland) supplemented with 10% FBS at 37 °C in a humidified atmosphere with 5% CO_2. Cells

https://doi.org/10.1021/acssensors.3c02268
ACS Sens. 2024, 9, 474−482

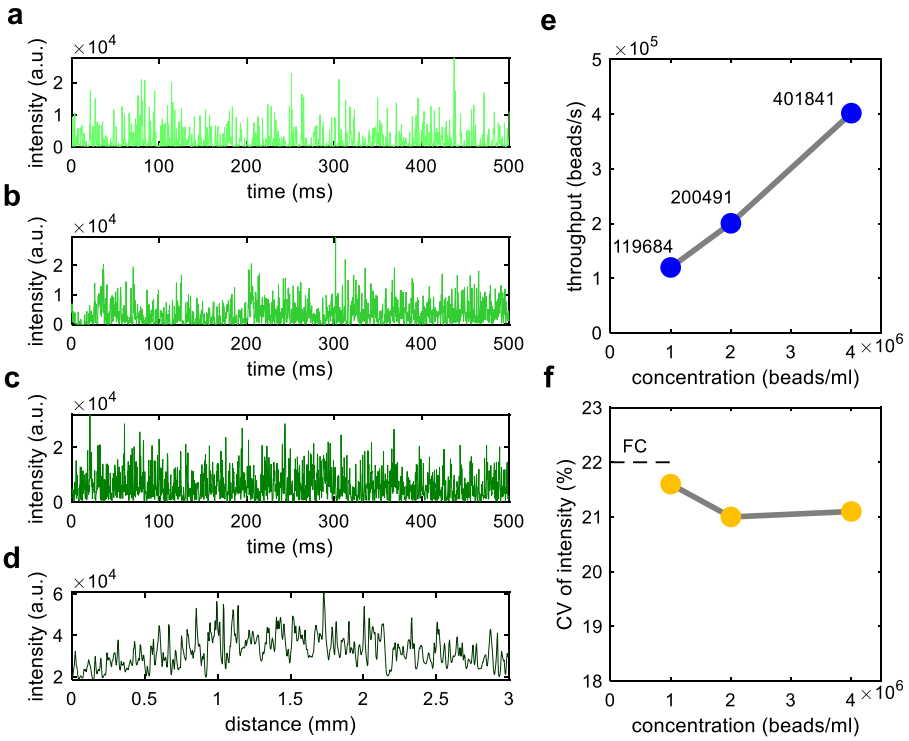

Figure 2. Characterization of RTCS throughput using 10 μm fluorescent beads. Fluorescent bead signals were recorded with the RTCS at concentrations of (a) 10^6, (b) 2×10^6, and (c) 4×10^6 beads/mL. Plots represent single-pixel readings of the CMOS image sensor as a function of time. (d) Single frame acquisition at a concentration of 5×10^6 beads/mL, highlighting significant overlap between the detected events. (e) Maximum RTCS throughput as a function of bead concentration between 10^6 and 4×10^6 beads/mL. Data points represent the average of three measurements. Error bars representing one standard deviation ($N = 3$) are smaller than the data symbols. (f) CV of intensity as a function of bead concentration. The dashed line reports the CV of intensity as measured using conventional FC. For bead concentrations higher than 1×10^6 beads/mL, the conventional flow cytometer does not provide accurate enumeration due to the occurrence of coincidence events, and thus, CV values cannot be obtained for the concentrations higher than 1×10^6 beads/mL. Data points represent the average of three measurements and error bars representing one standard deviation ($N = 3$) are smaller than the data points. The range of CV values (21−21.5%) at different bead concentrations is consistent with CV values measured using a commercial flow cytometer (22%).

were harvested by brief exposure to 0.25% trypsin/1 mM ethylenediaminetetraacetic acid (EDTA) (Thermo Fisher Scientific, Reinach, Switzerland). The cells were washed with 0.1% bovine serum albumin (BSA)/phosphate-buffered saline (PBS) and treated with 1 μg/mL Alexa Fluor 488 antihuman EGFR Ab (Biolegend, San Diego, USA) for 30 min at 4 °C and then washed with PBS. Fluorescence data were analyzed using a CytoFlex flow cytometer (Beckman Coulter, Pasadena, USA).

Optical Setup and Data Acquisition. The optical detection system consisted of an Eclipse Ti-E inverted microscope (Nikon, Zurich, Switzerland), integrating a motorized stage (Mad City Laboratories, Maddison, USA). 488 nm laser light (Coherent Genesis MX, Glasgow, UK) was focused into the microfluidic channel as a 15 μm-wide light sheet (similar to the average diameter of the cells under study) using a cylindrical lens (LJ1558RM-A, Thorlabs, Lübeck, Germany). Fluorescence photons were collected via a 4×/0.13 N.A. objective (Nikon, Zurich, Switzerland), passed through a 530 nm bandpass filter (F37-520, AHF, Tubingen, Germany) to reject the excitation light, and focused by a tube lens onto an S11639 CMOS linear sensor (Hamamatsu, Solothurn, Switzerland). An S13570 data acquisition printed circuit board (Hamamatsu, Solothurn, Switzerland) was used as a readout circuit. Acquired data were transferred to a PC via a USB 2.0 interface and processed with a custom-developed program written in C++ (Microsoft Visual Studio 2019) (Figure 1).

Microfluidic Device Operation. Bead and cell suspensions were prepared at various concentrations (10^6−10^7 beads/mL and 5×10^5−3×10^6 cells/mL, respectively) and loaded into 10 mL syringes (Hamilton Laboratory Products, Reno, USA). Suspensions were delivered into the microfluidic device using a precision syringe pump (neMESYS, Cetoni, Korbußen, Germany) at volumetric flow rates of 3 and 6 mL/min. The microfluidic device was placed on a motorized *xy* translation stage (Mad City Laboratories, Maddison, USA) to facilitate observation.

Viscoelastic polyethylene oxide (PEO) solutions were used to focus cells and beads at the image plane in a sheathless manner. When using viscoelastic carrier fluids, both inertial and viscoelastic forces control cell/particle migration. Specifically, two hydrodynamic forces (the elastic force and the inertial lift force) act on contained species and can be used to control particle trajectories. If the elastic and inertial forces are comparable, a 3D cell focusing at or near the channel centerline can be achieved. A detailed analysis of elasto-inertial focusing in such environments is provided elsewhere.[47,56] A stock solution of 1 MDa PEO (Sigma-Aldrich, Buchs, Switzerland) at a concentration of 10,000 ppm was prepared in Dulbecco's phosphate-buffered saline (DPBS, Life Technologies, Zug, Switzerland) and aged at room temperature for a month to enhance solution stability. For FC experiments, the stabilized PEO solution was diluted with DPBS, resulting in a final PEO concentration of 1000 ppm. Cell suspensions were mixed with 20% v/v OptiPrep Density Gradient Medium (Sigma-Aldrich, Buchs, Switzerland) to minimize cell sedimentation.

The maximum accessible frame rate of the CMOS sensor is 4000 frames/s and the horizontal field of view (FOV) of the sensor is 100 μm at 4× magnification. To ensure that each cell was imaged only once in each frame, cells should have a velocity, ν, equal to (FOV)/t, where t is the time between two consecutive frames. This time equates to 0.25 ms at a frame rate of 4000 frames/s, thus yielding a velocity of 0.4 m/s. This velocity corresponds to a volumetric flow rate of 6 mL/min, assuming a rectangular cross-section microfluidic channel. For experiments involving cells, longer exposure times were used to increase signal-to-noise ratios, and thus, volumetric flow rates

https://doi.org/10.1021/acssensors.3c02268
ACS Sens. 2024, 9, 474−482

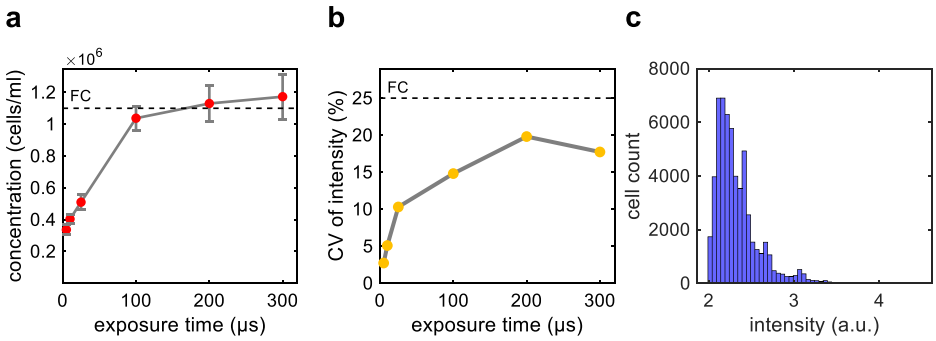

Figure 3. Optimization of the RTCS exposure time for the analysis of HEK cells at a concentration of 10^6 cells/mL. (a) Variation of HEK cell concentration measured using the RTCS as a function of exposure times between 6 and 300 μs. Exposure times above 100 μs yield sufficient sensitivity for detecting HEK cells. Concentrations measured with RTCS are in agreement with data extracted from conventional FC (horizontal dotted line). Data points represent the average of three measurements, with error bars representing one standard deviation ($N = 3$). (b) CV of the intensity as a function of exposure time between 6 and 300 μs. The CV value increases with exposure time up to 200 μs. Further increases in the exposure time result in a lower CV due to the motion blur. Data points represent the average of three measurements and error bars representing one standard deviation ($N = 3$) are smaller than the data points. (c) Representative intensity histogram of 56,501 HEK cells recorded for a period of 1 s using a 200 μs exposure time and a frame rate of 2000 frames/s.

were reduced to 3 mL/min to minimize motion blur. In this situation, the camera frame rate was reduced to 2000 frames/s to match the modified cell velocity of 0.2 m/s.

Real-Time Quantification. A custom program written in C++ using Microsoft Visual Studio 2019 was used to acquire and process raw sensor data. The program integrates a GUI with several functionalities, such as background acquisition, scaling of raw data, and the ability to display intensity histograms in real time. Since the excitation laser profile is not uniform across the channel cross-section, a non-uniform background signal will be present (Figure S1a). Accordingly, multiple signal processing operations are necessary to scale the raw data and correctly detect fluorescence signals. First, a background measurement was performed using the microfluidic channel filled with a 3 μM fluorescein isothiocyanate (FITC) (Sigma-Aldrich, Buchs, Switzerland) solution in DPBS. A cubic spline was applied to the intensity versus pixel number data to suppress local variations in the background signal (Figure S1b). These local variations were caused by statistical fluctuations of photons sensed at a specific exposure time and the dark current of the sensor. Scale factors were then calculated for each pixel and saved for use in the real-time detection algorithm. Sensor signals were then reconstructed by subtraction of the background signal. Fluorescence intensity peaks (associated with cells) were detected using a peak detection algorithm with minimum peak-to-peak distance and peak amplitude constraints (Figure S1c). The detected peaks were multiplied by the scale factors derived from the background signal (Figure S1d). Finally, fluorescence intensity histograms were displayed in real-time (with other metrics such as throughput and cell concentration). The exposure time, frame rate, and recording time are all adjustable via the GUI, with the program processing up to 4000 frames in real-time and saving 50,000 frames (corresponding to 12.5 s of recording time at 4000 frame/s).

■ RESULTS AND DISCUSSION

Ultrahigh-Throughput Quantification of Fluorescent Beads. To investigate the performance of the RTCS, commercial 10 μm diameter fluorescent beads (FC06F, PS/DVB-COOH (480,520), Bangs Laboratories, Indianapolis, USA) were used as model micron-sized species. Bead experiments were conducted at concentrations between 10^6 and 10^7 beads/mL. The average linear velocity of beads at a volumetric flow rate of 6 mL/min was calculated to be 0.4 m/s. Motion blur, D, can be simply defined as the product of shutter speed, t, and bead velocity, ν. In initial experiments, the exposure time was maintained at 6 μs, to minimize motion blur, but at the expense of reduced sensitivity. Under these conditions, motion blur was calculated to be 2.4 μm, which ensures adequate peak-to-peak separation between adjacent bead signals up to a concentration of 4×10^6 beads/mL (Figure 2a−c). Bead concentrations were measured using both the RTCS and a high-end flow cytometer (CytoFLEX, Beckman Coulter, Nyon, Switzerland) (Figures S2 and S3). As can be seen in Table S1, data collected using the RTCS at concentrations lower than 4×10^6 beads/mL were consistent with data obtained from conventional FC. The raw signals of an individual RTCS pixel as a function of time are shown in Figure 2a−c, with Figure 2d presenting raw signals from all pixels captured in a single frame for a concentration of 5×10^6 beads/mL. As the bead concentration increases from 10^6 to 4×10^6 beads/mL, the peak-to-peak separation of the intensity signals decreases, with signal peaks beginning to overlap at bead concentrations higher than 4×10^6 beads/mL (Figure 2d). This provides an upper concentration limit of 4×10^6 beads/mL using the current RTCS platform. Figure 2e presents analytical throughputs, as calculated from the intensity histograms shown in Figure S3, for the various bead concentrations. It can be seen that the RTCS exhibits a maximum real-time throughput of approximately 400,000 beads/s; a 40-fold improvement over high-end commercial flow cytometers, which can operate at throughputs of up to 10,000 cells/s at normal cell concentrations.[57] It should be noted that Fan et al.,[50] using an array of parallel channels and sheath flow focusing, predicted an "extrapolated" throughput of 1,000,000 cells/s (assuming concurrent operation of 32 parallel channels). That said, such an approach does not provide for real-time quantification and a maximum volumetric throughput of 0.33 mL/min is over 20 times lower than used in the RTCS. Finally, the coefficient of variation (CV), which defines the ratio of the standard deviation of fluorescence intensities of cells to the mean signal intensity, provides an excellent measure of relative variabilities in signal and is therefore useful when comparing the precision and sensitivity of different flow cytometers.[56] Using our RTCS, CV values (extracted from fluorescence intensity histograms) were between 21 and 21.5%; values consistent with the CV (22%) extracted from conventional FC (Figure 2f).

https://doi.org/10.1021/acssensors.3c02268
ACS Sens. 2024, 9, 474−482

Optimization of Exposure Time for Cellular Analysis. After optimizing conditions for the high-throughput analysis of micrometer-sized beads, the RTCS was used to assay fluorescent human embryonic kidney (HEK) cells. HEK cells have fluorescence quantum efficiencies significantly lower than those of fluorescent beads, with appreciable variations between individual cells. Accordingly, the exposure time was increased to allow for the efficient detection of all HEK cells within a heterogeneous population. Such an increase in exposure time enhances the detection sensitivity but comes at the expense of increased motion blur for a given flow velocity. To ensure minimal blur, the applied volumetric flow rate was decreased to 3 mL/min. This ensured adequate peak-to-peak separation but did reduce analytical throughput to approximately 75,000 cells/s. In initial experiments, the input cell concentration was fixed to 10^6 cells/mL, a value representative of typical concentrations used in a range of cell-based assays.[57] The exposure time was varied between 6 and 300 μs, with fluorescence intensity histograms being obtained at six exposure times. As can be seen in Figure 3a, cell concentrations measured using the RTCS were significantly different from concentrations extracted from conventional FC measurements when the exposure time was less than 100 μs, due to low sensitivity. However, for exposure times above 100 μs, the correspondence between the RTCS and FC data was excellent. Based on both concentration measurements and CV data (Figure 3b), 200 μs was selected as the optimum exposure time for cell experiments. A representative intensity histogram for HEK cells over a period of one s and with a 200 μs exposure time is shown in Figure 3c.

Sensitivity Characterization. The sensitivity of a flow cytometer can be assessed through its ability to quantify different levels of fluorescence emission. To assess the sensitivity of the RTCS, experiments were performed using Quantum Alexa Fluor 488 MESF calibration beads (Bangs Laboratories, Indianapolis, USA) that possess distinct and well-defined fluorescence intensities. Bead fluorescence was quantified in terms of MESF[58] (molecules of equivalent soluble fluorophores) units provided by the manufacturer. Specifically, four different calibration bead populations were used, with fluorescence intensities between 3179 and 333,766 MESF units (Figure S4a). Fluorescence intensities of the bead populations were measured with the RTCS and used to generate a calibration curve (Figure S4b) that reports RTCS intensities against manufacturer-specified intensity values. An excellent correlation between the experimental and manufacturer data is observed (R^2 = 0.9944). Significantly, the lowest fluorescence intensity bead population (#1), having an MESF unit intensity value of 3179, can be discriminated and clearly identified after background subtraction (Figure S5). Accordingly, a detection sensitivity of approximately 3000 MESF units can safely be assigned to our RTCS. Such a detection limit is significantly lower than needed for almost all applications in FC.[58]

Quantification of CTCs. The most used platform for CTC detection in clinical settings is the FDA-approved CellSearch system (Menarini Silicon Biosystems, Bologna, Italy). Detection relies on the expression of epithelial markers such as EpCAM (Epithelial Cell Adhesion Molecule) and PanCK (Pan-Cytokeratin) to capture and detect CTCs. Using this concept, and to assess the utility of the RTCS in CTC analysis, we mimicked CTCs using mNeonGreen labeled HEK cells and patient-derived human brain glioblastoma (LN229) cells labeled with Alexa Fluor 488 antihuman EGFR Ab, which were spiked into ten times diluted blood. The LN229 cancer cell was obtained from the University Hospital Zurich, and chosen because it is recognized to be representative of CTCs that can potentially be found in patients with brain glioblastoma.[59]

Blood samples were obtained from the Blutspende Zurich blood donation center. Six different cell suspensions were prepared by spiking HEK and LN229 cells into diluted blood at the ratios of 1/10,000, 1/100,000, and 1/1,000,000 (fluorescent cells to red blood cells). Figure 4 presents fluorescence intensity time traces generated from diluted whole blood containing HEK and LN229 cells at ratios of 1/10,000 over an 8 s time period. Single-cell events that correspond to strong and weak fluorescence signals can be clearly observed. CTCs are significantly more fluorescent than white and red blood cells. Accordingly, to detect CTCs, a detection threshold three times the standard deviation of the background signal was used. It should be noted that the threshold value can be fine-tuned depending on the sample under study. The numbers of red blood cells and fluorescent cells in each sample were additionally measured by conventional FC and are listed in Tables S2 and S3.

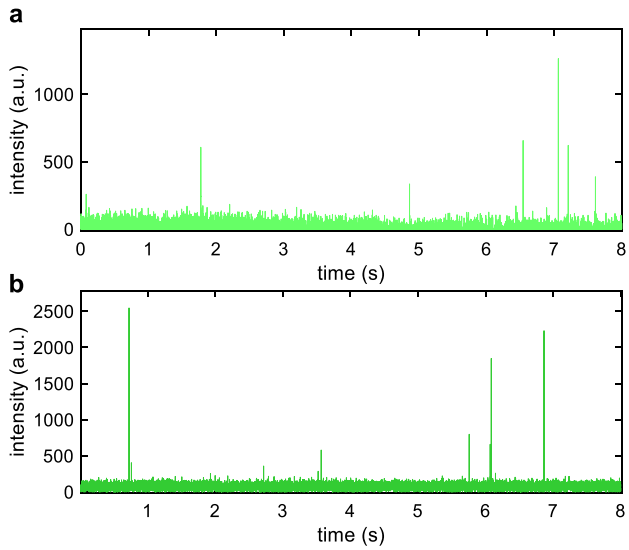

Figure 4. RTCS time trace for HEK and human glioblastoma (LN229) cells in diluted whole blood. Sensor readings for (a) HEK cells and (b) LN229 cells spiked into diluted whole blood using a 200 μs exposure time. Both samples were assayed for a period of 8 s, with single cells being observed as distinct, high-intensity peaks being above the noise level (3× the standard deviation) of the instrument. The background signal is subtracted from raw sensor data, and fluorescence intensity peaks of the individual cells are detected using the RTCS.

Figure 5 summarizes both conventional FC and RTCS analysis of the spiked HEK and LN229 cell suspensions. It can be seen that both methods yield almost identical measures of cell concentration under all conditions. However, it is critical to note that in this comparative analysis, conventional FC was performed at a flow rate of 60 μL/min (typical for normal operation) and using a 1000× dilution factor (to prevent cartridge blockage and coincident events detection). Significantly, the RTCS is able to quantify CTCs as rare as 6 CTCs per million red blood cells, using a volumetric flow rate of 3

https://doi.org/10.1021/acssensors.3c02268
ACS Sens. 2024, 9, 474−482

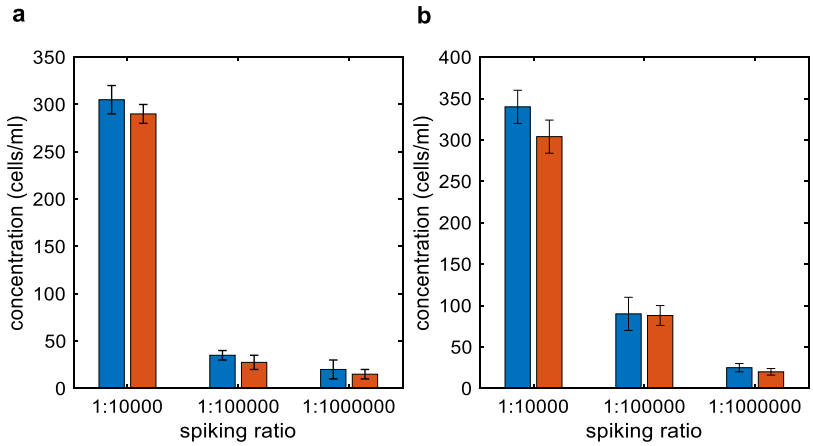

Figure 5. Rare cell quantification using conventional FC and the RTCS. (a) HEK cells spiked into diluted blood at ratios of 1/10,000, 1/100,000, and 1/1,000,000 measured by conventional FC (blue) and the RTCS (red). (b) Patient-derived CTCs (LN229 cells) spiked into diluted blood at ratios of 1/10,000, 1/100,000, and 1/1,000,000 measured by conventional FC (blue) and the RTCS (red). The RTCS data show a close correspondence to the FC data for all three spiking ratios. The height of each bar represents the average of three measurements, with error bars representing one standard deviation (N = 3).

mL/min and a 10× dilution factor (Figure 5a). To put this into context, using the microfluidic flow cytometer system presented by Zhao and co-workers,[7] CTCs could be screened at ratios as low as 2 cells per 1 mL of blood. However, the volumetric throughput of this system was only 80 μL/min, a value 40 times lower than the throughput achieved using the RTCS. Due to the high volumetric throughput of 3 mL/min, our RTCS is able to quantify CTCs contained in a 10 mL blood sample in just 5 min, rather than a typical 24 h time scale needed when using conventional FC or 18 h when using the fastest microfluidic cytometer.

CONCLUSIONS

To conclude, we have developed a real-time and ultrahigh-throughput fluorescence cytometer. The system consists of a linear CMOS image sensor with readout circuitry, an optical system, and a real-time particle quantification program. The program integrates a GUI able to acquire data, process fluorescence signals from flowing cells, and display intensity histograms in real time. Significantly, the RTCS is able to operate at exceptional analytical throughputs, of over 400,000 beads/s and 75,000 cells/s. These values represent a 40-fold and 7-fold improvement over high-end commercial flow cytometers. Additionally, the maximum volumetric throughput of the RTCS was 6 mL/min. This value is 60 times higher than the maximum flow rates used in conventional FC and crucially is high enough to enable rare cell analysis in blood within a few minutes. The real-time quantification capability is a key advantage of the RTCS when compared to other microflow cytometers that utilize post-data analysis. To showcase the utility of the RTCS in biological experimentation, CTC-spiked blood samples were assayed and quantified in a high-throughput manner, with the RTCS being able to detect CTCs at levels as low as 6 cells per one million blood cells. The sensitivity of the system was calculated to be 3190 MESF units by using commercial calibration beads. Accordingly, the RTCS allows for sensitive, high-throughput, and real-time detection of fluorescent particles and cells. Moreover, the system is simple to construct, easy to use, and applicable to point-of-care diagnostic applications. To this end, the RTCS has great potential as a rapid diagnostic platform, especially in resource-limited settings.

ASSOCIATED CONTENT

Supporting Information

The Supporting Information is available free of charge at https://pubs.acs.org/doi/10.1021/acssensors.3c02268.

Methods, supporting figures, and tables (PDF)

AUTHOR INFORMATION

Corresponding Authors

Stavros Stavrakis − *Institute for Chemical and Bioengineering, Department of Chemistry and Applied Biosciences, ETH Zürich, Zürich 8093, Switzerland;* orcid.org/0000-0002-0888-5953; Email: stavros.stavrakis@chem.ethz.ch

Andrew J. deMello − *Institute for Chemical and Bioengineering, Department of Chemistry and Applied Biosciences, ETH Zürich, Zürich 8093, Switzerland;* orcid.org/0000-0003-1943-1356; Email: andrew.demello@chem.ethz.ch

Authors

Mahmut Kamil Aslan − *Institute for Chemical and Bioengineering, Department of Chemistry and Applied Biosciences, ETH Zürich, Zürich 8093, Switzerland*

Yingchao Meng − *Institute for Chemical and Bioengineering, Department of Chemistry and Applied Biosciences, ETH Zürich, Zürich 8093, Switzerland;* orcid.org/0000-0001-9097-0868

Yanan Zhang − *Department of Neurology, University Hospital Zürich, 8091 Zürich, Switzerland; Clinical Neuroscience Center, University of Zürich, 8091 Zürich, Switzerland*

Tobias Weiss − *Department of Neurology, University Hospital Zürich, 8091 Zürich, Switzerland; Clinical Neuroscience Center, University of Zürich, 8091 Zürich, Switzerland*

Complete contact information is available at: https://pubs.acs.org/10.1021/acssensors.3c02268

Notes

The authors declare no competing financial interest.

https://doi.org/10.1021/acssensors.3c02268
ACS Sens. 2024, 9, 474−482

ACKNOWLEDGMENTS

This work was partially supported by a Strategic Focus Area Advanced Manufacturing grant and ETH Zurich.

REFERENCES

(1) Ignatiadis, M.; Sledge, G. W.; Jeffrey, S. S. Liquid Biopsy Enters the Clinic - Implementation Issues and Future Challenges. *Nat. Rev. Clin. Oncol.* **2021**, *18* (5), 297−312.

(2) Connal, S.; Cameron, J. M.; Sala, A.; Brennan, P. M.; Palmer, D. S.; Palmer, J. D.; Perlow, H.; Baker, M. J. Liquid Biopsies: The Future of Cancer Early Detection. *J. Transl. Med.* **2023**, *21* (1), 118.

(3) Castro-Giner, F.; Aceto, N. Tracking Cancer Progression: From Circulating Tumor Cells to Metastasis. *Genome Med.* **2020**, *12* (1), 31.

(4) Micalizzi, D. S.; Maheswaran, S.; Haber, D. A. A Conduit to Metastasis: Circulating Tumor Cell Biology. *Genes Dev.* **2017**, *31* (18), 1827−1840.

(5) Miller, M. C.; Doyle, G. V.; Terstappen, L. W. M. M. Significance of Circulating Tumor Cells Detected by the CellSearch System in Patients with Metastatic Breast Colorectal and Prostate Cancer. *J. Oncol.* **2010**, *2010*, 617421.

(6) Maheswaran, S.; Haber, D. A. Circulating Tumor Cells: A Window into Cancer Biology and Metastasis. *Curr. Opin. Genet. Dev.* **2010**, *20* (1), 96−99.

(7) Zhao, M.; Schiro, P. G.; Kuo, J. S.; Koehler, K. M.; Sabath, D. E.; Popov, V.; Feng, Q.; Chiu, D. T. An Automated High-Throughput Counting Method for Screening Circulating Tumor Cells in Peripheral Blood. *Anal. Chem.* **2013**, *85* (4), 2465−2471.

(8) Hartkopf, A. D.; Banys, M.; Krawczyk, N.; Wallwiener, M.; Schneck, H.; Neubauer, H.; Fehm, T. Circulating Tumor Cells in Early-Stage Breast Cancer. *Geburtshilfe Frauenheilkd.* **2011**, *71* (12), 1067−1072.

(9) Alunni-Fabbroni, M.; Sandri, M. T. Circulating Tumour Cells in Clinical Practice: Methods of Detection and Possible Characterization. *Methods* **2010**, *50* (4), 289−297.

(10) Dharmasiri, U.; Njoroge, S. K.; Witek, M. A.; Adebiyi, M. G.; Kamande, J. W.; Hupert, M. L.; Barany, F.; Soper, S. A. High-Throughput Selection, Enumeration, Electrokinetic Manipulation, and Molecular Profiling of Low-Abundance Circulating Tumor Cells Using a Microfluidic System. *Anal. Chem.* **2011**, *83* (6), 2301−2309.

(11) Lin, H. K.; Zheng, S.; Williams, A. J.; Balic, M.; Groshen, S.; Scher, H. I.; Fleisher, M.; Stadler, W.; Datar, R. H.; Tai, Y.-C.; Cote, R. J. Portable Filter-Based Microdevice for Detection and Characterization of Circulating Tumor Cells. *Clin. Cancer Res.* **2010**, *16* (20), 5011−5018.

(12) Kuo, J. S.; Zhao, Y.; Schiro, P. G.; Ng, L.; Lim, D. S. W.; Shelby, J. P.; Chiu, D. T. Deformability Considerations in Filtration of Biological Cells. *Lab Chip* **2010**, *10* (7), 837−842.

(13) Mohammadi, R.; Asghari, M.; Colombo, M.; Vaezi, Z.; Richards, D. A.; Stavrakis, S.; Naderi-Manesh, H.; deMello, A. Hybrid Microfluidic Device for High Throughput Isolation of Cells Using Aptamer Functionalized Diatom Frustules. *Chimia* **2022**, *76* (7−8), 661−668.

(14) Powell, A. A.; Talasaz, A. H.; Zhang, H.; Coram, M. A.; Reddy, A.; Deng, G.; Telli, M. L.; Advani, R. H.; Carlson, R. W.; Mollick, J. A.; Sheth, S.; Kurian, A. W.; Ford, J. M.; Stockdale, F. E.; Quake, S. R.; Pease, R. F.; Mindrinos, M. N.; Bhanot, G.; Dairkee, S. H.; Davis, R. W.; Jeffrey, S. S. Single Cell Profiling of Circulating Tumor Cells: Transcriptional Heterogeneity and Diversity from Breast Cancer Cell Lines. *PLoS One* **2012**, *7* (5), No. e33788.

(15) Kirby, B. J.; Jodari, M.; Loftus, M. S.; Gakhar, G.; Pratt, E. D.; Chanel-Vos, C.; Gleghorn, J. P.; Santana, S. M.; Liu, H.; Smith, J. P.; Navarro, V. N.; Tagawa, S. T.; Bander, N. H.; Nanus, D. M.; Giannakakou, P. Functional Characterization of Circulating Tumor Cells with a Prostate-Cancer-Specific Microfluidic Device. *PLoS One* **2012**, *7* (4), No. e35976.

(16) Nagrath, S.; Sequist, L. V.; Maheswaran, S.; Bell, D. W.; Irimia, D.; Ulkus, L.; Smith, M. R.; Kwak, E. L.; Digumarthy, S.; Muzikansky, A.; Ryan, P.; Balis, U. J.; Tompkins, R. G.; Haber, D. A.; Toner, M. Isolation of Rare Circulating Tumour Cells in Cancer Patients by Microchip Technology. *Nature* **2007**, *450* (7173), 1235−1239.

(17) Chudasama, D.; Barr, J.; Beeson, J.; Beddow, E.; McGonigle, N.; Rice, A.; Nicholson, A.; Anikin, V. Detection of Circulating Tumour Cells and Survival of Patients with Non-Small Cell Lung Cancer. *Anticancer Res.* **2017**, *37* (1), 169−173.

(18) Freydina, D. V.; Chudasama, D.; Freidin, M. B.; Leung, M.; Rice, A.; Montero Fernandez, A.; Nicholson, A. G.; Lim, E. Diagnostic Utility of Unbiased Circulating Tumour Cell Capture through Negative Depletion of Peripheral Blood Cells. *Oncology* **2015**, *89* (6), 360−364.

(19) Goodale, D.; Phay, C.; Postenka, C. O.; Keeney, M.; Allan, A. L. Characterization of Tumor Cell Dissemination Patterns in Preclinical Models of Cancer Metastasis Using Flow Cytometry and Laser Scanning Cytometry. *Cytometry, Part A* **2009**, *75* (4), 344−355.

(20) Takao, M.; Takeda, K. Enumeration, Characterization, and Collection of Intact Circulating Tumor Cells by Cross Contamination-Free Flow Cytometry. *Cytometry, Part A* **2011**, *79* (2), 107−117.

(21) Wang, N.; Shi, L.; Li, H.; Hu, Y.; Du, W.; Liu, W.; Zheng, J.; Huang, S.; Qu, X. Detection of Circulating Tumor Cells and Tumor Stem Cells in Patients with Breast Cancer by Using Flow Cytometry. *Tumor Biol.* **2012**, *33* (2), 561−569.

(22) Gronthos, S.; Franklin, D. M.; Leddy, H. A.; Robey, P. G.; Storms, R. W.; Gimble, J. M. Surface Protein Characterization of Human Adipose Tissue-Derived Stromal Cells. *J. Cell. Physiol.* **2001**, *189* (1), 54−63.

(23) McKinnon, K. M. Flow Cytometry: An Overview. *Curr. Protoc. Immunol.* **2018**, *120*, 5.1.1−5.1.11.

(24) Yang, A.-S.; Hsieh, W.-H. Hydrodynamic Focusing Investigation in a Micro-Flow Cytometer. *Biomed. Microdevices* **2007**, *9* (2), 113−122.

(25) Melamed, M. R. Chapter 1 A Brief History of Flow Cytometry and Sorting. In *Methods in Cell Biology*; Cytometry, 2001; Vol. *63*, pp 3−17.

(26) Kim, B.; Kang, D.; Choi, S. Handheld Microflow Cytometer Based on a Motorized Smart Pipette, a Microfluidic Cell Concentrator, and a Miniaturized Fluorescence Microscope. *Sensors* **2019**, *19* (12), 2761.

(27) Hong, B.; Zu, Y. Detecting Circulating Tumor Cells: Current Challenges and New Trends. *Theranostics* **2013**, *3* (6), 377−394.

(28) Donnenberg, A. D.; Meyer, E. M. Principles of Rare Event Analysis by Flow Cytometry: Detection of Injected Dendritic Cells in Draining Lymphatic Tissue. *Clin. Immunol. Newsl.* **1999**, *19* (10−11), 125−128.

(29) Piyasena, M. E.; Graves, S. W. The Intersection of Flow Cytometry with Microfluidics and Microfabrication. *Lab Chip* **2014**, *14* (6), 1044−1059.

(30) Shrirao, A. B.; Fritz, Z.; Novik, E. M.; Yarmush, G. M.; Schloss, R. S.; Zahn, J. D.; Yarmush, M. L. Microfluidic Flow Cytometry: The Role of Microfabrication Methodologies, Performance and Functional Specification. *Technology* **2018**, *6* (1), 1−23.

(31) Gong, Y.; Fan, N.; Yang, X.; Peng, B.; Jiang, H. New Advances in Microfluidic Flow Cytometry. *Electrophoresis* **2019**, *40*, 1212−1229.

(32) Bhagat, A. A. S.; Kuntaegowdanahalli, S. S.; Kaval, N.; Seliskar, C. J.; Papautsky, I. Inertial Microfluidics for Sheath-Less High-Throughput Flow Cytometry. *Biomed. Microdevices* **2010**, *12* (2), 187−195.

(33) McKenna, B. K.; Evans, J. G.; Cheung, M. C.; Ehrlich, D. J. A Parallel Microfluidic Flow Cytometer for High-Content Screening. *Nat. Methods* **2011**, *8* (5), 401−403.

(34) Lin, S.-C.; Yen, P.-W.; Peng, C.-C.; Tung, Y.-C. Single Channel Layer, Single Sheath-Flow Inlet Microfluidic Flow Cytometer with Three-Dimensional Hydrodynamic Focusing. *Lab Chip* **2012**, *12* (17), 3135−3141.

(35) Mao, X.; Nawaz, A. A.; Lin, S.-C. S.; Lapsley, M. I.; Zhao, Y.; McCoy, J. P.; El-Deiry, W. S.; Huang, T. J. An Integrated, Multiparametric Flow Cytometry Chip Using "Microfluidic Drifting"

Based Three-Dimensional Hydrodynamic Focusing. *Biomicrofluidics* **2012**, *6* (2), 24113−241139.
(36) Yang, R.-J.; Fu, L.-M.; Hou, H.-H. Review and Perspectives on Microfluidic Flow Cytometers. *Sens. Actuators, B* **2018**, *266*, 26−45.
(37) Lin, C.-H.; Lee, G.-B.; Fu, L.-M.; Hwey, B.-H. Vertical Focusing Device Utilizing Dielectrophoretic Force and Its Application on Microflow Cytometer. *J. Microelectromech. Syst.* **2004**, *13* (6), 923−932.
(38) Song, H.; Rosano, J. M.; Wang, Y.; Garson, C. J.; Prabhakarpandian, B.; Pant, K.; Klarmann, G. J.; Perantoni, A.; Alvarez, L. M.; Lai, E. Continuous-Flow Sorting of Stem Cells and Differentiation Products Based on Dielectrophoresis. *Lab Chip* **2015**, *15* (5), 1320−1328.
(39) Bruus, H.; Dual, J.; Hawkes, J.; Hill, M.; Laurell, T.; Nilsson, J.; Radel, S.; Sadhal, S.; Wiklund, M. Forthcoming Lab on a Chip Tutorial Series on Acoustofluidics: Acoustofluidics—Exploiting Ultrasonic Standing Wave Forces and Acoustic Streaming in Microfluidic Systems for Cell and Particle Manipulation. *Lab Chip* **2011**, *11* (21), 3579−3580.
(40) Ma, Z.; Zhou, Y.; Collins, D. J.; Ai, Y. Fluorescence Activated Cell Sorting via a Focused Traveling Surface Acoustic Beam. *Lab Chip* **2017**, *17* (18), 3176−3185.
(41) Mao, Z.; Xie, Y.; Guo, F.; Ren, L.; Huang, P.-H.; Chen, Y.; Rufo, J.; Costanzo, F.; Huang, T. J. Experimental and Numerical Studies on Standing Surface Acoustic Wave Microfluidics. *Lab Chip* **2016**, *16* (3), 515−524.
(42) Di Carlo, D.; Irimia, D.; Tompkins, R. G.; Toner, M. Continuous Inertial Focusing, Ordering, and Separation of Particles in Microchannels. *Proc. Natl. Acad. Sci. U.S.A.* **2007**, *104* (48), 18892−18897.
(43) Zhou, J.; Papautsky, I. Fundamentals of Inertial Focusing in Microchannels. *Lab Chip* **2013**, *13* (6), 1121−1132.
(44) Martel, J. M.; Toner, M. Inertial Focusing in Microfluidics. *Annu. Rev. Biomed. Eng.* **2014**, *16* (1), 371−396.
(45) Zhou, J.; Papautsky, I. Viscoelastic Microfluidics: Progress and Challenges. *Microsyst. Nanoeng.* **2020**, *6* (1), 113.
(46) Yang, S.; Kim, J. Y.; Lee, S. J.; Lee, S. S.; Kim, J. M. Sheathless Elasto-Inertial Particle Focusing and Continuous Separation in a Straight Rectangular Microchannel. *Lab Chip* **2011**, *11* (2), 266−273.
(47) Holzner, G.; Stavrakis, S.; deMello, A. Elasto-Inertial Focusing of Mammalian Cells and Bacteria Using Low Molecular, Low Viscosity PEO Solutions. *Anal. Chem.* **2017**, *89* (21), 11653−11663.
(48) Stavrakis, S.; Holzner, G.; Choo, J.; deMello, A. High-Throughput Microfluidic Imaging Flow Cytometry. *Curr. Opin. Biotechnol.* **2019**, *55*, 36−43.
(49) Fu, J.-L.; Fang, Q.; Zhang, T.; Jin, X.-H.; Fang, Z.-L. Laser-Induced Fluorescence Detection System for Microfluidic Chips Based on an Orthogonal Optical Arrangement. *Anal. Chem.* **2006**, *78* (11), 3827−3834.
(50) Fan, Y.-J.; Hsiao, Y.-C.; Weng, Y.-L.; Chen, Y.-H.; Chiou, P.-Y.; Sheen, H.-J. Development of a Parallel Three-Dimensional Microfluidic Device for High-Throughput Cytometry. *Sens. Actuators, B* **2020**, *320*, 128255.
(51) Hur, S. C.; Tse, H. T. K.; Carlo, D. D. Sheathless Inertial Cell Ordering for Extreme Throughput Flow Cytometry. *Lab Chip* **2010**, *10* (3), 274−280.
(52) Diebold, E. D.; Buckley, B. W.; Gossett, D. R.; Jalali, B. Digitally Synthesized Beat Frequency Multiplexing for Sub-Millisecond Fluorescence Microscopy. *Nat. Photonics* **2013**, *7* (10), 806−810.
(53) Psaltis, D.; Quake, S. R.; Yang, C. Developing Optofluidic Technology through the Fusion of Microfluidics and Optics. *Nature* **2006**, *442* (7101), 381−386.
(54) Seo, S.; Su, T.-W.; Tseng, D. K.; Erlinger, A.; Ozcan, A. Lensfree Holographic Imaging for On-Chip Cytometry and Diagnostics. *Lab Chip* **2009**, *9* (6), 777−787.
(55) Seo, S.; Isikman, S. O.; Sencan, I.; Mudanyali, O.; Su, T.-W.; Bishara, W.; Erlinger, A.; Ozcan, A. High-Throughput Lens-Free Blood Analysis on a Chip. *Anal. Chem.* **2010**, *82* (11), 4621−4627.
(56) Holzner, G.; Mateescu, B.; Van Leeuwen, D.; Cereghetti, G.; Dechant, R.; Stavrakis, S.; deMello, A. High-Throughput Multiparametric Imaging Flow Cytometry: Toward Diffraction-Limited Sub-Cellular Detection and Monitoring of Sub-Cellular Processes. *Cell Rep.* **2021**, *34* (10), 108824.
(57) Cossarizza, A.; Chang, H.-D.; Radbruch, A.; Akdis, M.; Andrä, I.; Annunziato, F.; Bacher, P.; Barnaba, V.; Battistini, L.; Bauer, W. M.; Baumgart, S.; Becher, B.; Beisker, W.; Berek, C.; Blanco, A.; Borsellino, G.; Boulais, P. E.; Brinkman, R. R.; Büscher, M.; Busch, D. H.; Bushnell, T. P.; Cao, X.; Cavani, A.; Chattopadhyay, P. K.; Cheng, Q.; Chow, S.; Clerici, M.; Cooke, A.; Cosma, A.; Cosmi, L.; Cumano, A.; Dang, V. D.; Davies, D.; De Biasi, S.; Del Zotto, G.; Della Bella, S.; Dellabona, P.; Deniz, G.; Dessing, M.; Diefenbach, A.; Di Santo, J.; Dieli, F.; Dolf, A.; Donnenberg, V. S.; Dörner, T.; Ehrhardt, G. R. A.; Endl, E.; Engel, P.; Engelhardt, B.; Esser, C.; Everts, B.; Dreher, A.; Falk, C. S.; Fehniger, T. A.; Filby, A.; Fillatreau, S.; Follo, M.; Förster, I.; Foster, J.; Foulds, G. A.; Frenette, P. S.; Galbraith, D.; Garbi, N.; García-Godoy, M. D.; Geginat, J.; Ghoreschi, K.; Gibellini, L.; Goettlinger, C.; Goodyear, C. S.; Gori, A.; Grogan, J.; Gross, M.; Grützkau, A.; Grummitt, D.; Hahn, J.; Hammer, Q.; Hauser, A. E.; Haviland, D. L.; Hedley, D.; Herrera, G.; Herrmann, M.; Hiepe, F.; Holland, T.; Hombrink, P.; Houston, J. P.; Hoyer, B. F.; Huang, B.; Hunter, C. A.; Iannone, A.; Jäck, H.; Jávega, B.; Jonjic, S.; Juelke, K.; Jung, S.; Kaiser, T.; Kalina, T.; Keller, B.; Khan, S.; Kienhöfer, D.; Kroneis, T.; Kunkel, D.; Kurts, C.; Kvistborg, P.; Lannigan, J.; Lantz, O.; Larbi, A.; LeibundGut-Landmann, S.; Leipold, M. D.; Levings, M. K.; Litwin, V.; Liu, Y.; Lohoff, M.; Lombardi, G.; Lopez, L.; Lovett-Racke, A.; Lubberts, E.; Ludewig, B.; Lugli, E.; Maecker, H. T.; Martrus, G.; Matarese, G.; Maueröder, C.; McGrath, M.; McInnes, I.; Mei, H. E.; Melchers, F.; Melzer, S.; Mielenz, D.; Mills, K.; Mirrer, D.; Mjösberg, J.; Moore, J.; Moran, B.; Moretta, A.; Moretta, L.; Mosmann, T. R.; Müller, S.; Müller, W.; Münz, C.; Multhoff, G.; Munoz, L. E.; Murphy, K. M.; Nakayama, T.; Nasi, M.; Neudörfl, C.; Nolan, J.; Nourshargh, S.; O'Connor, J.-E.; Ouyang, W.; Oxenius, A.; Palankar, R.; Panse, I.; Peterson, P.; Peth, C.; Petriz, J.; Philips, D.; Pickl, W.; Piconese, S.; Pinti, M.; Pockley, A. G.; Podolska, M. J.; Pucillo, C.; Quataert, S. A.; Radstake, T. R. D. J.; Rajwa, B.; Rebhahn, J. A.; Recktenwald, D.; Remmerswaal, E. B. M.; Rezvani, K.; Rico, L. G.; Robinson, J. P.; Romagnani, C.; Rubartelli, A.; Ruckert, B.; Ruland, J.; Sakaguchi, S.; Sala-de-Oyanguren, F.; Samstag, Y.; Sanderson, S.; Sawitzki, B.; Scheffold, A.; Schiemann, M.; Schildberg, F.; Schimisky, E.; Schmid, S. A.; Schmitt, S.; Schober, K.; Schüler, T.; Schulz, A. R.; Schumacher, T.; Scotta, C.; Shankey, T. V.; Shemer, A.; Simon, A.-K.; Spidlen, J.; Stall, A. M.; Stark, R.; Stehle, C.; Stein, M.; Steinmetz, T.; Stockinger, H.; Takahama, Y.; Tarnok, A.; Tian, Z.; Toldi, G.; Tornack, J.; Traggiai, E.; Trotter, J.; Ulrich, H.; van der Braber, M.; van Lier, R. A. W.; Veldhoen, M.; Vento-Asturias, S.; Vieira, P.; Voehringer, D.; Volk, H.-D.; von Volkmann, K.; Waisman, A.; Walker, R.; Ward, M. D.; Warnatz, K.; Warth, S.; Watson, J. V.; Watzl, C.; Wegener, L.; Wiedemann, A.; Wienands, J.; Willimsky, G.; Wing, J.; Wurst, P.; Yu, L.; Yue, A.; Zhang, Q.; Zhao, Y.; Ziegler, S.; Zimmermann, J. Guidelines for the Use of Flow Cytometry and Cell Sorting in Immunological Studies. *Eur. J. Immunol.* **2017**, *47* (10), 1584−1797.
(58) Wang, L.; Gaigalas, A. K.; Abbasi, F.; Marti, G. E.; Vogt, R. F.; Schwartz, A. Quantitating Fluorescence Intensity From Fluorophores: Practical Use of MESF Values. *J. Res. Natl. Inst. Stand. Technol.* **2002**, *107* (4), 339−353.
(59) Müller, C.; Holtschmidt, J.; Auer, M.; Heitzer, E.; Lamszus, K.; Schulte, A.; Matschke, J.; Langer-Freitag, S.; Gasch, C.; Stoupiec, M.; Mauermann, O.; Peine, S.; Glatzel, M.; Speicher, M. R.; Geigl, J. B.; Westphal, M.; Pantel, K.; Riethdorf, S. Hematogenous Dissemination of Glioblastoma Multiforme. *Sci. Transl. Med.* **2014**, *6* (247), 247ra101.